A novel micro-computerized tomography method reveals *Drosophila* cardiac hypertrophy caused by upregulated store-operated calcium entry

Courtney E Petersen[1], Todd A Schoborg[2], and Jeremy T Smyth[3*]

[1]Graduate Program in Molecular and Cell Biology and [3]Department of Anatomy, Physiology, and Genetics, Uniformed Services University of the Health Sciences, F. Edward Hébert School of Medicine, Bethesda, MD 20814

[2]Department of Molecular Biology, University of Wyoming, Laramie, WY 82017

[*]Corresponding Author:

Jeremy T Smyth
Uniformed Services University of the Health Sciences
4301 Jones Bridge Rd
Bethesda, MD 20814
Tel: (301) 295-5879
Email: jeremy.smyth@usuhs.edu

ABSTRACT

Heart failure is often preceded by pathological cardiac hypertrophy, a thickening of the heart musculature driven by complex gene regulatory and signaling processes. The *Drosophila* heart has great potential as a genetic model for deciphering the mechanisms that underlie cardiac hypertrophy. However, current methods for evaluating hypertrophy of the *Drosophila* heart are laborious and difficult to carry out reproducibly. Here we demonstrate that micro-computerized tomography (microCT) is an accessible, highly reproducible method for non-destructive, quantitative analysis of the morphology and size of the *Drosophila* heart. To validate our microCT approach for analyzing *Drosophila* cardiac hypertrophy, we show that expression of constitutively active Ras (*Ras85D*^{V12}), previously shown to cause hypertrophy of the fly heart, results in significant thickening of both adult and larval heart walls when measured from microCT images. We then show using microCT analysis that genetic upregulation of store-operated Ca^{2+} entry (SOCE) driven by expression of constitutively active Stim (Stim^{CA}) or Orai (Orai^{CA}) proteins also results in significant hypertrophy of the *Drosophila* heart, through a process that specifically depends on Ca^{2+} influx through Orai channels. Importantly, dysregulation of Ca^{2+} homeostasis in cardiomyocytes is a major driver of cardiac hypertrophy, but the underlying mechanisms are unclear. These results demonstrate that increased SOCE activity is an important driver of hypertrophic cardiomyocyte growth, and demonstrate how microCT analysis combined with tractable genetic tools in *Drosophila* can be used to delineate molecular signaling processes that underlie cardiac hypertrophy and heart failure.

INTRODUCTION

Pathological cardiac hypertrophy occurs when the heart enlarges in response to conditions of chronic functional overload, such as hypertension or valve stenosis. This enlargement is initially compensatory to increase cardiac output in response to the underlying pathology. However, unmitigated hypertrophy eventually transitions to irreversible fibrosis of the heart musculature, stiffening of the ventricular walls, and decreased luminal diameter, resulting in impaired systolic function and reduced cardiac output (4; 32; 54; 57). Pathological cardiac hypertrophy almost invariably progresses to heart failure, a major cause of death worldwide (17; 31). Despite significant advances in treatment, there are no cures for pathological cardiac hypertrophy or heart failure, demonstrating a critical need for better understanding of the cellular and molecular mechanisms that contribute to maladaptive cardiomyocyte growth.

A mechanistic hallmark of pathological cardiac hypertrophy is reactivation of fetal gene expression pathways in cardiomyocytes (10; 23; 28). Several key signaling processes are upregulated in cardiomyocytes from hypertrophic hearts, resulting in increased expression of cardiac contractility and growth genes including β-myosin heavy chain (β-MHC), myosin light chain 1/3 (MLC1/3), and atrial and brain natriuretic peptides (ANP and BNP) (22; 23). One of the most prominent of these signaling pathways is the Ca^{2+} – calcineurin – NFAT axis, whereby enhanced Ca^{2+} cycling in cardiomyocytes activates the NFAT transcription factor via the Ca^{2+}/calmodulin-regulated phosphatase calcineurin (6; 8; 36; 51; 56). Importantly, calcineurin activation is both necessary and sufficient for pathological cardiac hypertrophy in mammalian models (18; 36; 60), and calcineurin signaling has emerged as an attractive therapeutic target for anti-hypertrophic drugs. However, the mechanisms that lead to enhanced Ca^{2+} cycling in hypertrophic cardiomyocytes are poorly understood. Moreover, signaling pathways involving phosphatidylinositol 4,5-bisphosphate kinase (PI3K), Ras and Raf small GTPases, nitric oxide, and Ca^{2+}/calmodulin-dependent protein kinases (CaMKs) are also essential mediators of

hypertrophic cardiomyocyte growth (1; 14; 54), but integration of these signaling processes is highly complex and poorly understood. Resolution of this complexity will benefit greatly from molecular pathway dissection in a genetically tractable model like *Drosophila melanogaster*.

Drosophila has become firmly established as an important model organism for understanding the developmental genetic and signaling processes that regulate heart physiology. The *Drosophila* heart is a linear tube of cardiomyocytes that runs along the dorsal midline of the animal and pumps hemolymph, a lymph-like fluid, throughout the body in an open circulatory system (45; 47; 53). Importantly, *Drosophila* cardiomyocyte physiology is highly conserved with mammals, allowing for relevant comparative analyses of the genetic and functional bases of cardiomyopathies (7; 26; 39; 40; 45). A major advantage of *Drosophila* over mammalian models in cardiac research is the ability to quickly and easily engineer multiple genetic alterations in the same animal for integrated signaling pathway analysis. These approaches have shown that both the Ras-Raf-MAPK and calcineurin-regulated signaling pathways drive cardiac hypertrophy in *Drosophila* (25; 64; 65), demonstrating that hypertrophic signaling in the fly heart is well conserved with mammals. However, the full potential of *Drosophila* for deciphering conserved mechanisms of cardiac hypertrophy has been limited by a lack of readily accessible and reproducible methods for analyzing fly heart wall thickness.

Prior analyses of *Drosophila* cardiac hypertrophy have relied on histopathology (25; 62; 63; 65), which involves fixing and embedding whole flies, physical sectioning along the length of the heart tube, and microscopic imaging of individual sections to directly measure heart wall dimensions. This approach has several drawbacks that can limit throughput, reproducibility, and accuracy. First, it is very time-consuming and laborious, and this limits the feasibility of processing large numbers of samples required for genetic pathway analyses. Second, achieving consistent sectioning through the same regions of the heart and in the same orientation between samples is challenging, and this is critical for reproducibility of measurements. Third,

physical sectioning through the heart yields relatively thick sections of 8-10μm, and this can limit the accuracy of individual measurements.

Several recent studies have described the use of micro-computerized tomography (microCT) for quantitative analysis of internal organs and structures in *Drosophila* (15; 16; 30; 34; 35; 50), and a major goal of our current study was to determine whether microCT is an effective tool for analysis of cardiac hypertrophy in flies. MicroCT is an x-ray based imaging platform in which the sample is incrementally rotated to generate a series of images that encompasses the full sample volume. Computerized algorithms are then used to generate three-dimensional (3D) reconstructions or tomograms of the entire sample. When applied to whole *Drosophila* larvae, pupae, or adults, microCT allows visualization of internal organs in any orientation and at any location within the specimen with unprecedented clarity and resolution (50). And importantly, microCT imaging is isotropic, so measurements made in any dimension or orientation can be directly compared. Thus, with microCT, measurements can be reproducibly made from the same location within a specific organ or structure without reliance on imprecise physical sectioning. MicroCT also involves relatively simple fixation and staining protocols, with the ability to process multiple animals at a time. Reproducible measurements of *Drosophila* heart wall thickness have been made using microCT (50); however, whether microCT can be used to analyze pathological changes to heart morphology and architecture such as hypertrophy has not been determined. Importantly, integration of microCT analysis with combinatorial *Drosophila* genetic tools may provide powerful insight into molecular mechanisms of pathological heart remodeling.

Here we demonstrate that analytical microCT approaches can accurately and reproducibly report hypertrophy of the *Drosophila* heart. As proof-of-principle, we first show using microCT that expression of a constitutively active Ras mutant, previously shown to cause cardiac hypertrophy in *Drosophila* by histopathological analyses (64), results in significantly

increased heart wall thickness in adult flies. We then apply additional genetic approaches and microCT analysis to demonstrate that upregulation of store-operated Ca^{2+} entry (SOCE) drives cardiac hypertrophy in *Drosophila*. SOCE is a highly conserved Ca^{2+} signaling mechanism that couples influx of extracellular Ca^{2+} to the depletion of endo/sarcoplasmic reticulum (E/SR) Ca^{2+} stores. SOCE is mediated by Ca^{2+} sensing Stim proteins in the E/SR and Orai Ca^{2+} influx channels in the plasma membrane (3; 46; 52). Accumulating evidence suggests that SOCE upregulation in cardiomyocytes is necessary and sufficient for pressure-overload induced cardiac hypertrophy, likely due to direct SOCE activation of calcineurin signaling (9; 19; 58). However, mechanisms that regulate SOCE in cardiomyocytes, and how SOCE signaling integrates with other hypertrophic signaling processes are largely unknown. Our study demonstrates that by combining microCT analysis with robust genetic tools in *Drosophila*, we can carry out highly reproducible analyses of hypertrophic signaling mechanisms that are driven by upregulated SOCE. This microCT approach to analyzing cardiac hypertrophy is straightforward, accessible, and readily adaptable to the renowned genetic tools in *Drosophila*, creating a powerful experimental platform for delineating the complex cellular and genetic processes that drive pathological cardiac hypertrophy.

MATERIALS AND METHODS

Fly Stocks

The following *Drosophila* stocks were obtained from the Bloomington *Drosophila* Stock Center: W1118 (3605), *UAS-Ras85D*^{V12} (64195), and Orai RNAi (53333). *tinC-GAL4* was obtained from Dr. Manfred Frausch (Friedrich Alexander University). CM-tdTom flies were obtained from Dr. Rolf Bodmer (Sanford Burnham Prebys Institute). Wildtype *Orai* (*Orai*^{WT}) and constitutively active *Orai* (*Orai*^{CA}) were obtained from Dr. Gaiti Hasan (National Center for Biological Sciences, Bangalore, India). Orai^{CA} has a glycine to methionine mutation at amino acid position 170 (68). To generate *UAS-Stim-GFP* flies, plasmid LD45776 containing the cDNA sequence of *Drosophila Stim* Isoform A was obtained from the *Drosophila* Genomics Resource Center. The *Stim* coding sequence was cloned by PCR and inserted into vector pPWG (Carnegie *Drosophila* Gateway Vector Collection), which introduces a C-terminal EGFP tag and upstream *UASp* promoter. This vector was then sent to Bestgene for embryo injection and selection of transgenic animals. To generate constitutively active *Stim* (*UAS-Stim*^{CA}) animals, site-directed mutagenesis (Stratagene QuikChange XL Kit) was used to change aspartic acids at positions 155 and 157 to alanines using the *UAS-Stim-GFP* described above as template. Sequence confirmed plasmid was then sent to BestGene for embryo injection and selection of transformants.

Micro-computerized Tomography (microCT)

The following microCT methods were adapted from protocols published by Schoborg et al (49; 50):

Adult Labeling

5-20 adult flies were anesthetized with CO_2 and transferred to a 1.5mL Eppendorf tube containing 1ml of phosphate buffered saline + 0.5% Triton-X 100 (0.5% PBST). Tubes

were capped and gently inverted, then incubated for 5 min at room temperature to remove the wax cuticle. Flies were then transferred to tubes containing 1ml Bouin's fixative solution (5% acetic acid, 9% formaldehyde, 0.9% picric acid; Sigma) for 24 hours. Samples were washed 3x30 min on a shaker in 1 ml μCT Wash Buffer (0.1M Na_2HPO_4/NaH_2P0_4 + 1.8% Sucrose, pH 7.0), followed by staining with 1ml of 0.1N iodine-iodide solution (Lugol's solution) for 48hrs. Flies were then washed with two changes of ultrapure water and stored at room temperature for up to one month prior to scanning.

Larval Labeling

Third instar, wandering larvae were collected and placed in 1.5 ml Eppendorf tube with 1 ml 0.5% PBST. Tubes were then placed on a 100°C heat block for 20 seconds, followed by cooling at room temperature for 5 mins. Larvae were then fixed in Bouin's solution for 24 hours and washed as described for adults. Prior to labeling with Lugol's solution, larval cuticles were punctured at their anterior and posterior ends with a microdissection needle, avoiding areas with underlying soft tissue, to allow penetration of the labeling solution. Punctured larvae were then incubated in Lugol's solution for 48 hrs, washed with two changes of ultrapure water, and stored at room temperature for up to one month prior to scanning.

Sample Mounting and Scanning

Individual adult and larval samples were placed head-down in heat sealed 10 μl micropipette tips containing ultrapure water, and a dulled 20-guage needle was used to gently lower the animals until they fit snuggly in the taper of the pipette tip. Parafilm was wrapped around base of micropipette tip to prevent water leakage. Mounted samples

were secured to the stage of the microCT scanner, pipette base down, using mounting putty. Samples were scanned with a Bruker SkyScan 1172 desktop scanner controlled by Skyscan software (Bruker) operated on a Dell workstation computer. The following X-ray source voltage and current settings were used: 40kV, 110 μA, and 4 W. A Hamamatsu 10 Mp camera with 11.54 μm pixel size coupled to a scintillator was used to collect X-rays and convert to photons. Fast scans utilized a medium camera resolution setting of 2.85 μm, and slow, high-resolution scans used a small camera resolution setting of 1.15 μm with 360 degrees of sample rotation. Frame averaging was set to four for all scans.

Reconstruction

Tomograms were generated using NRecon software (Bruker MicroCT, v1.7.0.4). The built-in shift correction function of NRecon, which uses reference scans to compensate for sample movement during scanning (e.g., thermal fluctuations or slowly varying sample movements), was used for image alignment and reconstruction. Any remaining misalignment was manually fine-tuned using the misalignment compensation function. Ring artifact correction was set to max (50) and beam hardening was set to 0%.

Heart Wall Thickness Measurements

Fully reconstructed microCT tomogram image series were imported into ImageJ (NIH) and viewed using the Orthogonal Views function to locate and orient the heart in XY, XZ, and YZ orientations. The conical chamber of the heart is located in the anterior-most region of the abdomen and can be easily identified in images in which the last segments of the thoracic muscles are visible. Using images that showed the largest opening of the conical chamber in cross section, lines were drawn through the thickest sections of the

lateral heart walls and lengths of the lines recorded in μm. An average of ten measurements from five slices was then used to represent each animal.

Intravital Fluorescence Microscopy

Intravital fluorescence imaging of adult hearts was carried out using animals that express tdTomato under control of the cardiomyocyte-specific R94C02 (CM-tdTom) enhancer element (21) as previously described (44). Five-day old adult females were briefly anesthetized with CO_2 and adhered dorsal side down to a glass coverslip with Norland Optical Adhesive that was then cured with a 48-watt UV LED light source (LKE) for 60 seconds. Animals were allowed to recover for 10 mins prior to imaging. The heart was imaged through the dorsal cuticle at a rate of 200 frames per second (fps) for twenty seconds using an ORCA-Flash4.0 V3 sCMOS camera (Hamamatsu) on a Nikon Ti2 inverted microscope controlled with Nikon Elements software. Excitation light at 550 nm was provided by a Spectra-X illuminator (Lumencor) and emission was collected through a 555-635 nm band-pass filter. To generate M-modes, a 1-pixel wide line was drawn through the heart chamber in the A2 segment, and the fluorescence intensity along this line for the full time-course was plotted using ImageJ. End diastolic dimensions (EDD) and end systolic dimensions (ESD) were calculated directly from the processed M-mode traces by manually measuring the distance between the heart walls at full relaxation and full contraction, respectively. An average of five measurements of EDD and ESD was calculated from each trace. Heart rate was calculated by manually counting the number of systoles over 20 seconds. FS was calculated as ((EDD-ESD) / EDD) x 100.

Developmental Timing

Approximately 30-40 virgin female *tinC-GAL4* or *W1118* animals were mated with males carrying specified transgenes under *UAS* control for three days, at which time animals were transferred into egg laying chambers that consisted of a 100 ml plastic beaker with holes for air

exchange affixed over a petri dish containing grape juice agar (Genesee Scientific). A dollop of yeast paste (active dry yeast mixed with water) was placed in the center of each grape juice agar plate as food. Animals were acclimated in the chambers for 24 hours, and then transferred to new plates for 4 hours at 25ºC for timed egg laying. After removing adults, plates with eggs were incubated at 25ºC for an additional 24 hours. Hatched larvae were then transferred to vials with standard fly food, with up to 30 larvae per vial, and maintained at 25ºC over the course of the experiment. Vials were checked each day, and the numbers of newly formed pupae and eclosed adults were recorded.

Statistical Analyses

All statistical analyses were carried out using GraphPad Prism software. Contractility parameters and heart wall measurements were analyzed by One-way ANOVA followed by Tukey's Multiple Comparisons Test. Differences were considered statistically significant at $p < 0.05$.

RESULTS

Effective microCT analysis of cardiac hypertrophy in Drosophila larvae and adults

Direct measurements of heart wall thickness to analyze cardiac hypertrophy in *Drosophila* have previously been done using histopathological methods. These methods rely on mechanical tissue sectioning and microscopic imaging of individual tissue slices, making it difficult and laborious to acquire reproducible measurements from the same region of the heart between samples. Recent reports have demonstrated that microCT can non-invasively generate complete, 3-dimensional isometric image sets encompassing the entire *Drosophila* body in which all major internal organs, including the heart, can be clearly visualized. We therefore reasoned that microCT could be used to non-destructively image the entire *Drosophila* heart, allowing for reproducible heart wall measurements along the length of the heart tube. We began by analyzing hearts in adult flies. Based on published protocols, whole intact adult flies were fixed in Bouin's solution and labeled with iodine to achieve sufficient X-ray attenuation of soft tissues. We then imaged adults by microCT at the highest resolution settings for which the entire animal still fits within the detector's field of view (1.15 μm/pixel). Acquired tomograms produced a fully reconstructed animal (Figure 1A), and the entire heart tube, running anterior to posterior along the dorsal abdominal wall, is clearly visible in longitudinal views from high-resolution image stacks (Figure 1B). As previously described, these images have exceptional resolution that is sensitive enough to identify discrete structures such as ostia (50). To distinctly delineate the heart walls, we focused on the conical chamber at the anterior-most end of the heart where the heart chamber is largest, and the heart walls have the greatest separation. We then generated cross-sectional views from this region. As shown in Figure 1C and D, cross-sectional views from the conical chamber provided clear visualization of the heart walls around the complete circumference of the heart. Image sets from high-resolution scans provide superior visualization of heart structure and morphology. However, these scans require 4-6 hours to

complete and are thus not practical to generate large datasets for quantitative analysis. Instead, scans of the entire adult fly at a lower resolution of 2.85 µm/pixel can be completed in approximately 30 minutes, such that multiple animals can be scanned in several hours. As shown in Figure 1E and F, the heart walls can still be clearly delineated in low-resolution cross-sections of the conical chamber, though the margins are not as sharp. Importantly, low resolution images can be used to directly measure the thickness of the heart walls, and measurements from low-resolution scans of 22 *W1118* control adults indicated a mean heart wall thickness in the conical chamber of 7.97 ± 0.13 µm (mean ± SEM; Figure 1G). Importantly, heart wall thickness measurements obtained from microCT scans were nearly identical to previously published measurements from histopathological preparations (25; 64; 65). Moreover, the low variance of our measurements suggests the microCT-based methodology has a high degree of reproducibility.

We next determined whether our microCT-based approach can accurately detect hypertrophy of the adult *Drosophila* heart. We tested this by expressing a constitutively active mutant of Ras (*Ras85D*^{V12}) that has previously been shown to induce cardiac hypertrophy in flies (64). As shown in Figure 1C and D, heart-specific expression of *Ras85D*^{V12} using the *tinC-GAL4* driver resulted in noticeable thickening of the heart walls and reduced luminal area in high-resolution cross-section images of the conical chamber compared to *W1118* controls. Direct measurements from low-resolution images (Figure 1E and F) revealed a significant increase in heart wall thickness of approximately 33% in *Ras85D*^{V12} compared to *W1118* control hearts (Figure 1G). These results demonstrate that microCT imaging is a robust method for detection and analysis of hypertrophy of the *Drosophila* heart.

Drosophila heart development shares many similarities with the early stages of vertebrate heart development, and analysis of the *Drosophila* heart during developmental stages like larvae may therefore prove invaluable for our understanding of human heart

development and congenital heart defects (40; 47; 59). Additionally, the majority of cardiomyocyte growth in *Drosophila* occurs during the larval stage of development, which makes the larval heart a useful model for studying mechanisms that regulate both physiological and pathological heart growth (37; 45). We therefore assessed the use of microCT to evaluate heart wall thickness in larva, and whether changes in thickness are detectable with this method. The heart spans approximately the posterior third of the third-instar larva and is situated just under the dorsal cuticle (Figures 2 A-D). Heart wall measurements made along the lateral sides of the heart tube in low-resolution cross-sectional images of *W1118* controls revealed a thickness of 7.24 ± 0.10 μm (mean ± SEM; Figure 2 E-G). Similar to adults, heart specific expression of $Ras85D^{V12}$ resulted in a modest but highly reproducible and significant increase in larval heart wall thickness of approximately 26% compared to *W1118* controls (Figure 2G). Collectively, these results demonstrate that microCT generates images of *Drosophila* larvae and adults with sufficient resolution and sensitivity to allow for accurate analysis of small changes in delicate tissues like the heart. Furthermore, we show that the combination of microCT with *Drosophila* genetic tools is a powerful analytical approach for studying mechanisms of cardiac hypertrophy.

SOCE upregulation results in pathological cardiac hypertrophy

Heart specific upregulation of SOCE is required for the induction pathological cardiac hypertrophy in vertebrate models (9; 19; 27; 55; 58). However, mechanisms that regulate SOCE in cardiomyocytes are still poorly understood. *Drosophila* may serve as an important model to elucidate how SOCE regulates cardiac hypertrophy, but whether SOCE upregulation results in hypertrophy of the *Drosophila* heart has yet to be determined. We therefore used microCT analysis to evaluate whether SOCE upregulation due to expression of constitutively active *Stim* and *Orai* mutants in *Drosophila* results in increased heart wall thickness. Constitutively active Stim ($Stim^{CA}$) contains two aspartic acid to alanine substitutions within the EF-hand domain,

rendering Stim unable to bind ER luminal Ca^{2+} (66). Constitutively active Orai ($Orai^{CA}$) has a glycine to methionine mutation in the hinge region of the channel, forcing the channel into an open conformation (68). As shown in Figure 3, heart specific expression of $Stim^{CA}$ and $Orai^{CA}$ resulted in significantly increased heart wall thickness compared to *W1118* controls as well as animals expressing wildtype *Stim* and *Orai* constructs ($Stim^{WT}$ and $Orai^{WT}$, respectively). Thickening of the heart walls in $Stim^{CA}$ and $Orai^{CA}$ expressing animals was comparable to increases observed with $Ras85D^{V12}$ expression (Figure 3C and D), demonstrating that our results with $Stim^{CA}$ and $Orai^{CA}$ are consistent with an established model of *Drosophila* cardiac hypertrophy.

Reactivation of signaling mechanisms that drive cardiomyocyte growth during heart development is a hallmark of pathological cardiac hypertrophy (10). In accordance with this, mammalian STIM1 and Orai1 have high expression levels during fetal development that drop precipitously into adulthood, but are restored upon induction of pathological cardiac hypertrophy (8; 19; 27; 58). This suggests that SOCE signaling may be essential for developmental cardiomyocyte growth; however, little is known regarding the role of SOCE in cardiac development. We therefore determined whether SOCE upregulation results in increased heart wall thickness in larvae using microCT. Similar to adults, heart specific expression of $Stim^{CA}$ resulted in significantly increased heart wall thickness in third-instar larvae compared to *W1118* controls, as well as to larvae expressing $Stim^{WT}$ (Figure 4). Increased larval heart wall thickness by $Stim^{CA}$ expression was again similar to thickening caused by $Ras85D^{V12}$ expression (Figure 4B). Thus, SOCE upregulation drives aberrant growth of the *Drosophila* heart during larval development as well as in adult animals.

SOCE upregulation impairs heart contractility

Cardiac hypertrophy impairs heart contractility and suppresses cardiac output due to reduced heart wall flexibility and chamber volume (4; 32; 57). Therefore, we next evaluated

whether SOCE upregulation due to *Stim*^{CA} and *Orai*^{CA} expression affects heart contractility. Adult heart contractility was analyzed by intravital fluorescence imaging of animals with cardiomyocyte-specific tdTomato (CM-tdTom) expression (21; 44). As shown in Figure 5A-D, control hearts exhibited strong, consistent contractions with an average end diastolic dimension (EDD) of 65.17 ± 1.33 μm, average end systolic dimension (ESD) of 32.15 ± 0.83 μm, and average fractional shortening (FS) of 51 ± 0.85% (mean ± SEM). These parameters were not significantly altered by expression of *Stim*^{WT} or *Orai*^{WT}. In striking contrast, M-mode traces from *Stim*^{CA}, *Orai*^{CA}, and *Ras85D*^{V12} expressing hearts showed visibly narrowed diastolic dimensions (Figure 5A), and direct EDD measurements were significantly reduced compared to controls by 26%, 32%, and 15% for *Stim*^{CA}, *Orai*^{CA}, and *Ras85D*^{V12}, respectively (Figure 5B). ESD was also significantly reduced in *Stim*^{CA}, *Orai*^{CA}, and *Ras85D*^{V12} expressing hearts (Figure 5C), whereas FS was unaltered in *Stim*^{CA} or *Orai*^{CA} and in fact modestly increased in *Ras85D*^{V12} expressing hearts (Figure 5D). Heart rate was reduced in *Ras85D*^{V12} hearts but was unchanged by *Stim*^{CA} and *Orai*^{CA} expression (Figure 5E). Importantly, reduced EDD is indicative of impaired relaxation while reduced ESD suggests decreased luminal volume, both of which are serious contractile impairments typically seen in hypertrophic hearts. Thus, these results demonstrate that SOCE upregulation results in contractile dysfunction consistent with cardiac hypertrophy observed in microCT analyses. Notably, the effects of SOCE upregulation on heart structure and function were pathological, as the number of heart-specific *Stim*^{CA} expressing animals reaching the pupal stage of development (pupariation) was reduced by approximately 70% compared to controls, and only about 20% of *Stim*^{CA} animals reached adulthood (Supplemental Figure 1).

Stim*^{CA}*-mediated hypertrophy and impaired contractility specifically require Orai channels

It has been suggested that in addition to Orai channels, Stim proteins regulate Orai-independent targets in cardiomyocytes including L-type Ca^{2+} channels and phospholamban (42;

67). We therefore determined whether hypertrophy and impaired contractility caused by $Stim^{CA}$ expression specifically required Orai channels. To evaluate this, we generated animals that co-express $Stim^{CA}$ with *Orai* RNAi specifically in cardiomyocytes. As shown in Figure 6A and C, microCT analysis again showed significant thickening of heart walls in animals with heart specific $Stim^{CA}$ expression alone. Strikingly however, the hypertrophic phenotype was completely suppressed by co-expression of *Orai* RNAi with $Stim^{CA}$, as heart wall thickness in these animals was similar to controls as well as to animals with *Orai* RNAi alone. This strongly suggests that hypertrophy of $Stim^{CA}$ expressing hearts results from upregulated Ca^{2+} influx through Orai channels. This conclusion is further supported by our finding that hypertrophy caused by $Ras85D^{V12}$ expression was not suppressed by co-expression of *Orai* RNAi (Figure 6 B and D). Thus, the ability of Orai knockdown to suppress hypertrophy is specific to the effects of SOCE upregulation, as opposed to a generalized ability of Orai suppression to universally repress hypertrophic growth.

Additionally, we determined whether the effects of $Stim^{CA}$ expression on heart contractility similarly depend on Orai channels. In support of this, co-expression of *Orai* RNAi with $Stim^{CA}$ reverted the reductions in EDD, ESD, and heart rate seen with $Stim^{CA}$ expression alone (Figure 7A and C-F). The effect of *Orai* suppression was again specific to $Stim^{CA}$, as reductions in EDD, ESD, and heart rate caused by $Ras85D^{V12}$ expression were unchanged by co-expression with *Orai* RNAi (Figure 7B and G-J) and in fact, EDD and ESD were further reduced compared to $Ras85D^{V12}$ alone. These results collectively demonstrate that SOCE upregulation in *Drosophila* drives cardiac hypertrophy and pathologically impairs contractile heart function. Importantly, the effects of SOCE upregulation are specific and distinct from other mechanisms that drive hypertrophic growth of the heart, such as upregulation of Ras signaling..

DISCUSSION

Cardiac growth and remodeling are essential for proper heart development and the ability to respond to physiological or pathological increases in functional demand, such as pregnancy and exercise or myocardial infarction and hypertension, respectively (4; 11; 33; 61) Experimental approaches that combine molecular genetics with *in vivo* analysis of heart architecture and function are essential for understanding both physiological and pathological heart remodeling and hypertrophy. Here we have demonstrated that microCT is an accessible and powerful non-destructive imaging platform for analysis of *Drosophila* heart architecture that, when combined with genetic tools and functional heart analysis, can be used to decipher complex mechanisms of heart growth and pathological remodeling. Our introduction of microCT imaging to the *Drosophila* heart analysis toolkit has the potential to significantly accelerate our understanding of the conserved genetic and signaling mechanisms that regulate heart development, and that are re-engaged during pathological hypertrophy and heart failure.

The *Drosophila* heart is a valuable model for understanding the molecular etiology of cardiomyopathies and heart failure. *Drosophila* have been widely used to study dilated cardiomyopathy, likely because dilated cardiomyopathy can be readily assessed based solely on relatively straightforward contractility analyses. Few studies, on the other hand, have analyzed cardiac hypertrophy in flies. Notably, a finding of cardiac hypertrophy requires not only altered contractility, but also direct measurements indicating increased heart wall thickness. These measurements are challenging in flies due to the small size and delicate tissue of the fly heart. Accordingly, the most common approach, histopathological preparation, is time intensive and adversely affected by differences in tissue sectioning and mounting. We now show that microCT can yield heart size measurements in flies that are rapidly obtained, highly reproducible, and sensitive enough to detect changes in heart wall thickness indicative of hypertrophy. Another distinct advantage of microCT over histopathology is that microCT

generates complete 3D reconstructions of the whole animal, such that the entire heart and other internal tissues and organs can be visualized in various orientations and perspectives. Thus, multiple landmarks external to the heart can be used to orient consistent measurements of the heart between animals. Furthermore, prolonged cardiac disease and heart failure have the potential to profoundly impact the physiology of other organs, such as skeletal muscle and renal function (20). Simultaneous analysis of multiple organs in the same animal with microCT therefore holds immense and relatively unmatched potential for the study of multifactorial diseases that affect the heart in addition to other organs.

We first validated our microCT approach for detection of *Drosophila* cardiac hypertrophy by analyzing animals that express constitutively active Ras, an established model of cardiac hypertrophy in flies based on histopathological analysis (64). Importantly, our microCT measurements of heart wall thickness in adult controls were consistent with measurements made from histopathological preparations, indicating a normal thickness of about 6-8μm. Constitutively active *Ras85D*^{V12} expression resulted in a 3-4μm, or approximately 50%, increase compared to controls by our microCT measurements, indicating significant hypertrophy. Notably however, prior histopathological measurements showed an approximately 15 μm increase in thickness with *Ras85D*^{V12} expression (64). A possible reason for this difference is that histopathological measurements were made from transverse heart sections that were 8 μm thick, whereas our microCT measurements were made from 2.85 μm optical slices. We expect that the smaller sections used for microCT measurements will result in more accurate, though potentially smaller measurements of heart wall thickness. It is also possible that our *Ras85D*^{V12} expression was not as penetrant as in previous studies. Of note, Yu et al. reported that heart-specific *Ras85D*^{V12} expression resulted in significantly reduced eclosion and poor survival of adult escapers, whereas we did not observe significant effects of *Ras85D*^{V12} expression on animal development or survival (not shown).

We have also demonstrated the utility of microCT for analysis of the larval *Drosophila* heart. This is significant, because the majority of physiological heart growth in *Drosophila* occurs during the larval stages of animal development (40; 45; 47). Thus, application of microCT to larval heart analysis may be a valuable tool for delineating physiological mechanisms of developmental heart growth. And given that many of these developmental growth mechanisms are re-activated during pathological cardiac hypertrophy and heart failure, microCT analysis of the larval heart may prove an essential tool for uncovering new mechanisms that drive heart failure as well (10; 18).

MicroCT has been largely underutilized for analysis of *Drosophila* anatomy and physiology, particularly when combined with other established genetic and imaging approaches. To demonstrate the power of microCT for analysis of signaling pathways that drive cardiac hypertrophy, we used this technique to investigate the role of SOCE signaling in hypertrophy of the *Drosophila* heart. Numerous studies have demonstrated that upregulated SOCE is essential for the induction of pathological cardiac hypertrophy (2; 19; 27; 43; 58). However, we still have much to learn about the precise roles of SOCE signaling in hypertrophic cardiomyocyte growth. Furthermore, individuals with gain-of-function mutations in human STIM1 and Orai1 have not presented with cardiac phenotypes (24), further highlighting significant gaps in our understanding of SOCE function in the heart. Thus, a genetic model of upregulated SOCE activity may prove vital to understanding the mechanisms by which SOCE regulates cardiac physiology and disease pathogenesis. Our microCT data clearly show that genetic upregulation of SOCE function in cardiomyocytes by expression of constitutively active *Stim* or *Orai* mutants results in significant thickening of the *Drosophila* heart, similar to heart wall thickening caused by $Ras85D^{V12}$ expression. And importantly, we combined microCT measurements with direct, *in vivo* analysis of heart contractility by intravital imaging to determine the effect of hypertrophy caused by SOCE upregulation on heart function. Consistent with the hypertrophic phenotype

that restrict the inner dimensions of the heart chamber, *Stim*^{CA} and *Orai*^{CA} as well as *Ras85D*^{V12} expression resulted in significantly reduced diastolic and systolic dimensions. These results establish a new genetic model of SOCE-mediated cardiac hypertrophy that, when combined with other genetic analyses in *Drosophila*, may prove vital for delineating the integrated role of SOCE signaling in cardiac disease pathogenesis. These results also demonstrate the power of integrating microCT analysis in flies with other measures of heart architecture and contractility for understanding the complex relationship between heart form and function.

The consistency of our microCT and contractility results between both *Stim*^{CA} and *Orai*^{CA} expression suggest a specific role for Stim/Orai mediated SOCE in cardiac hypertrophy, as opposed to SOCE-independent functions of Stim and Orai that have been previously demonstrated (12; 38; 48). This conclusion is further supported by our result showing that hypertrophy caused by Stim^{CA} expression specifically requires Orai channels, whereby Orai suppression reversed the hypertrophic effects of Stim^{CA} expression. Notably, this was not the case for *Ras85D*^{V12}-induced hypertrophy, as Orai suppression had no effect. Thus, Orai suppression does not have a generalized anti-hypertrophic effect. This result also suggests that Ras and Stim/Orai-mediated SOCE function in parallel hypertrophic signaling pathways, as opposed to a linear pathway in which Ras functions upstream of Stim and Orai.

Previous findings in mammalian models suggest that upregulation of wildtype STIM1 expression, as opposed to a constitutively active STIM1 mutant, is sufficient for induction of cardiac hypertrophy and heart failure (9). Our results, however, indicate that wildtype Stim expression alone is not sufficient for hypertrophy of the *Drosophila* heart. One possible reason for this difference is that our expression levels of transgenic Stim in cardiomyocytes is not high enough to drive hypertrophy. It is also possible that the stoichiometry of Stim and Orai expression in *Drosophila* cardiomyocytes may differ from mammals. For example, if native Stim expression in *Drosophila* cardiomyocytes is already stoichiometrically matched to Orai

expression, then increasing Stim expression may not significantly affect SOCE function without a compensatory increase in Orai expression. Furthermore, Orai1-independent targets of STIM1, including canonical transient receptor potential (TrpC) channels (13; 29; 41; 48), L-type Ca^{2+} channels (42), and phospholambans (67), may also contribute to STIM1-dependent cardiac hypertrophy in mammals, whereas our results suggest that Stim functions specifically through Orai channels to drive *Drosophila* cardiac hypertrophy. Thus, there may be differences between Stim and Orai function in mammalian versus *Drosophila* cardiomyocytes related to stoichiometry and/or functional targets. Importantly though, *Drosophila* offers a more simplified model in which we can focus our analyses specifically on Stim and Orai mediated SOCE function in cardiac hypertrophy independently of SOCE-independent functions.

Accumulating evidence suggests that SOCE-mediated Ca^{2+} influx acts through calcineurin signaling to drive hypertrophic cardiomyocyte growth and impaired heart contractility (2; 9; 19; 27). However, additional targets of upregulated SOCE in cardiomyocytes have also been reported. For example, increased STIM1 expression in hypertrophied cat and mouse hearts is associated with enhanced CaMKII (9) activity and mTORC2/Akt (2) signaling that may also contribute to the hypertrophic phenotype (9; 55). Transgenic upregulation of STIM1 has also been shown to enhance Ca^{2+} spark frequencies and generate spontaneous action potentials in mammalian cardiomyocytes (5; 9; 55; 58). Furthermore, defects in mitochondrial structure including increased fragmentation and loss of crista structure were also noted in transgenic STIM1 mouse hearts (9). Thus, consistent with the complex and multi-faceted etiology of pathological cardiac hypertrophy, the role of SOCE in this disease process likely involves multiple targets and regulatory processes. Advanced genetic tools coupled with microCT and contractility analyses in *Drosophila* will serve as a valuable experimental platform for deciphering the complex pathophysiology of pathological cardiac hypertrophy and heart failure.

FIGURE LEGENDS

<u>Figure 1:</u> MicroCT analysis of normal and hypertrophied hearts in adult *Drosophila*

A. Maximum intensity projection of the full, high-resolution microCT image series of a 7-day old W1118 adult female fly, providing a 3D representation of the whole animal. The yellow line indicates the location of the cross-section images used for heart wall measurements. **B.** Single longitudinal microCT image through the center of a 7-day old *W1118* adult female fly imaged at high resolution. Yellow arrow indicates the conical chamber of heart. **C.** Single cross-section high-resolution microCT images at the thorax to abdomen transition and bisecting the conical chamber, from 7-day old *W1118* (left) and *tinC-GAL4* driven *Ras85D*^{V12} adult female flies. Yellow boxes denote the conical chambers of the hearts. **D.** Expanded images of the regions within the yellow boxes in C, showing magnification of the conical chambers. **E.** Single cross-section low-resolution microCT images at the thorax to abdomen transition and bisecting the conical chamber, from the same 7-day old *W1118* (left) and *tinC-GAL4* driven *Ras85D*^{V12} adult female flies shown in C. Yellow boxes denote the conical chambers of the hearts. **F.** Expanded images of the regions within the yellow boxes in E, showing magnification of the conical chambers. Yellow lines on heart walls indicate areas where heart wall measurements were made. **G.** Plot of heart wall measurements taken from low-resolution microCT scans of *W1118* and *tinC-GAL4* driven *Ras85D*^{V12} 7-day old adult females. Each symbol represents an average of ten measurements from a single animal. Bars indicate mean ± s.e.m., and p-values calculated from One-way ANOVA with Tukey's Multiple Comparison.

<u>Figure 2:</u> MicroCT analysis of normal and hypertrophied hearts in third instar *Drosophila* larvae

A. Maximum intensity projection of the full, high-resolution microCT image series of a 3rd instar larva, providing a 3D representation of the whole animal. The yellow line indicates the location of the cross-section images used for heart wall measurements. **B.** Single longitudinal microCT image through the center of a 3rd instar larva imaged at high resolution. Yellow arrowhead indicates the heart. **C.** Single cross-section high-resolution microCT image bisecting the heart from the high-resolution microCT scans represented in B. The yellow box surrounds the heart and denotes the region expanded in **D.** to show the heart at higher magnification. **E.** Single cross-section low-resolution microCT images from the posterior of *W1118* (left) and *tinC-GAL4* driven *Ras85D*^{V12} 3rd instar larvae. The yellow box surrounds the heart and denote the regions expanded in **F.** to show the hearts at higher magnification. Yellow lines in **F** indicate areas where heart wall measurements were made. **G.** Plot of heart wall measurements taken from low-resolution microCT scans of *W1118* and *tinC-GAL4* driven *Ras85D*^{V12} 3rd instar larvae. Each symbol represents an average of ten measurements from a single animal. Bars indicate mean ± s.e.m., and p-values calculated from One-way ANOVA with Tukey's Multiple Comparison.

<u>Figure 3:</u> SOCE upregulation results in hypertrophy of adult *Drosophila* hearts.

A-B. Representative cross-section low-resolution microCT images of the abdomen to thorax transition, cropped to show conical chambers of 7-day old adult females with *tinC-GAL4* and *W1118* (control), and *tinC-GAL4* driven Stim^{WT}, Stim^{CA}, and *Ras85D*^{V12} (**A**), and with *tinC-GAL4* and CM-tdTom (control), and *tinC-GAL4* driven Orai^{WT}, and Orai^{CA} (**B**). **C-D.** Plots of heart wall measurements taken from low-resolution microCT scans of 7-day old adult females with the

genotypes shown in A and B, respectively. Each symbol represents an average of ten measurements from a single animal. Bars indicate mean ± s.e.m., and p-values calculated from One-way ANOVA with Tukey's Multiple Comparison.

<u>Figure 4:</u> SOCE upregulation results in hypertrophy of larval *Drosophila* hearts.

A. Representative cross section low-resolution microCT images from the posterior of 3rd instar larvae, cropped to show the hearts from animals with *tinC-GAL4* and *W1118* (control), and *tinC-GAL4* driven $Stim^{WT}$, $Stim^{CA}$, and $Ras85D^{V12}$ **B.** Plot of heart wall measurements taken from low-resolution microCT scans of 3rd instar larvae with the genotypes shown in A. Each symbol represents an average of ten measurements from a single animal. Bars indicate mean ± s.e.m., and p-values calculated from One-way ANOVA with Tukey's Multiple Comparison.

<u>Figure 5:</u> SOCE upregulation results in altered heart contractility with reduced heart chamber dimensions.

A. Heart contractility was analyzed by intravital imaging of 5-day old adult females expressing CM-tdTom. Shown are representative M-mode traces from animals with *tinC-GAL4* and CM-tdTom (control), and *tinC-GAL4* driven $Stim^{WT}$, $Orai^{WT}$, $Stim^{CA}$, $Orai^{CA}$, and $Ras85D^{V12}$. The red line in the CM-tdTom trace depicts systole and the yellow line depicts diastole. **B-E.** Plots of EDD (**B**), ESD (**C**), FS (**D**), and HR (**E**) calculated from M-mode traces of the genotypes shown in A. Each symbol represents an average of five measurements from a single animal. Bars indicate mean ± s.e.m., and p-values were calculated from One-way ANOVA with Tukey's Multiple Comparison.

<u>Figure 6:</u> Cardiac hypertrophy caused by constitutively active Stim expression requires Orai channels.

A-B. Representative cross-section low-resolution microCT images of the abdomen to thorax transition, cropped to show conical chambers of 7-day old adult females with *tinC-GAL4* and CM-tdTom (control), and *tinC-GAL4* driven Orai RNAi, $Stim^{CA}$, and Orai RNAi plus $Stim^{CA}$ (**A**), and *tinC-GAL4* and CM-tdTom (control), and *tinC-GAL4* driven Orai RNAi, $Ras85D^{V12}$, and Orai RNAi plus $Ras85D^{V12}$ (**B**). **C-D.** Plots of heart wall measurements taken from low-resolution microCT scans of 7-day old adult females with the genotypes shown in A and B, respectively. Each symbol represents an average of ten measurements from a single animal. Bars indicate mean ± s.e.m., and p-values calculated from One-way ANOVA with Tukey's Multiple Comparison.

<u>Figure 7:</u> Altered heart contractility caused by constitutively active Stim expression requires Orai channels.

A-B. Representative M-mode traces from intravital imaging of 7-day old adult females with *tinC-GAL4* and CM-tdTom (control), and *tinC-GAL4* driven Orai RNAi, $Stim^{CA}$, and Orai RNAi plus $Stim^{CA}$ (**A**), and *tinC-GAL4* and CM-tdTom (control), and *tinC-GAL4* driven Orai RNAi, $Ras85D^{V12}$, and Orai RNAi plus $Ras85D^{V12}$ (**B**). **C-J.** Plots of EDD (**C,G**), ESD (**D,H**), FS (**E,I**), and HR (**F,J**) calculated from M-mode traces of the genotypes shown in A and B. Each symbol represents an average of five measurements from a single animal. Bars indicate mean ± s.e.m., and p-values were calculated from One-way ANOVA with Tukey's Multiple Comparison.

REFERENCES

1. Backs J, Song K, Bezprozvannaya S, Chang S, Olson EN. 2006. CaM kinase II selectively signals to histone deacetylase 4 during cardiomyocyte hypertrophy. *The Journal of clinical investigation* 116:1853-64

2. Benard L, Oh JG, Cacheux M, Lee A, Nonnenmacher M, et al. 2016. Cardiac Stim1 Silencing Impairs Adaptive Hypertrophy and Promotes Heart Failure Through Inactivation of mTORC2/Akt Signaling. *Circulation* 133:1458-71; discussion 71

3. Berna-Erro A, Woodard GE, Rosado JA. 2012. Orais and STIMs: physiological mechanisms and disease. *Journal of cellular and molecular medicine* 16:407-24

4. Bernardo BC, Weeks KL, Pretorius L, McMullen JR. 2010. Molecular distinction between physiological and pathological cardiac hypertrophy: experimental findings and therapeutic strategies. *Pharmacology & therapeutics* 128:191-227

5. Bonilla IM, Belevych AE, Baine S, Stepanov A, Mezache L, et al. 2019. Enhancement of Cardiac Store Operated Calcium Entry (SOCE) within Novel Intercalated Disk Microdomains in Arrhythmic Disease. *Scientific reports* 9:10179

6. Bueno OF, Wilkins BJ, Tymitz KM, Glascock BJ, Kimball TF, et al. 2002. Impaired cardiac hypertrophic response in Calcineurin Abeta -deficient mice. *Proceedings of the National Academy of Sciences of the United States of America* 99:4586-91

7. Choma MA, Suter MJ, Vakoc BJ, Bouma BE, Tearney GJ. 2011. Physiological homology between Drosophila melanogaster and vertebrate cardiovascular systems. *Disease models & mechanisms* 4:411-20

8. Collins HE, Zhu-Mauldin X, Marchase RB, Chatham JC. 2013. STIM1/Orai1-mediated SOCE: current perspectives and potential roles in cardiac function and pathology. *American journal of physiology. Heart and circulatory physiology* 305:H446-58

9. Correll RN, Goonasekera SA, van Berlo JH, Burr AR, Accornero F, et al. 2015. STIM1 elevation in the heart results in aberrant Ca(2)(+) handling and cardiomyopathy. *Journal of molecular and cellular cardiology* 87:38-47

10. Dirkx E, da Costa Martins PA, De Windt LJ. 2013. Regulation of fetal gene expression in heart failure. *Biochimica et biophysica acta* 1832:2414-24

11. Dorn GW, 2nd. 2007. The fuzzy logic of physiological cardiac hypertrophy. *Hypertension (Dallas, Tex. : 1979)* 49:962-70

12. Eder P. 2017. Cardiac Remodeling and Disease: SOCE and TRPC Signaling in Cardiac Pathology. *Advances in experimental medicine and biology* 993:505-21

13. Eder P, Molkentin JD. 2011. TRPC channels as effectors of cardiac hypertrophy. *Circulation research* 108:265-72

14. Erickson JR. 2014. Mechanisms of CaMKII Activation in the Heart. *Frontiers in pharmacology* 5:59

15. Fabian B, Schneeberg K, Beutel RG. 2016. Comparative thoracic anatomy of the wild type and wingless (wg(1)cn(1)) mutant of Drosophila melanogaster (Diptera). *Arthropod structure & development* 45:611-36

16. Harrison JF, Waters JS, Biddulph TA, Kovacevic A, Klok CJ, Socha JJ. 2018. Developmental plasticity and stability in the tracheal networks supplying Drosophila flight muscle in response to rearing oxygen level. *Journal of insect physiology* 106:189-98

17. Heidenreich PA, Albert NM, Allen LA, Bluemke DA, Butler J, et al. 2013. Forecasting the impact of heart failure in the United States: a policy statement from the American Heart Association. *Circulation. Heart failure* 6:606-19

18. Heineke J, Molkentin JD. 2006. Regulation of cardiac hypertrophy by intracellular signalling pathways. *Nature reviews. Molecular cell biology* 7:589-600

19. Hulot JS, Fauconnier J, Ramanujam D, Chaanine A, Aubart F, et al. 2011. Critical role for stromal interaction molecule 1 in cardiac hypertrophy. *Circulation* 124:796-805

20. Jackson G, Gibbs CR, Davies MK, Lip GY. 2000. ABC of heart failure. Pathophysiology. *BMJ* 320:167-70

21. Klassen MP, Peters CJ, Zhou S, Williams HH, Jan LY, Jan YN. 2017. Age-dependent diastolic heart failure in an in vivo Drosophila model. *eLife* 6

22. Kohli S, Ahuja S, Rani V. 2011. Transcription factors in heart: promising therapeutic targets in cardiac hypertrophy. *Current cardiology reviews* 7:262-71

23. Kuwahara K, Nishikimi T, Nakao K. 2012. Transcriptional regulation of the fetal cardiac gene program. *Journal of pharmacological sciences* 119:198-203

24. Lacruz RS, Feske S. 2015. Diseases caused by mutations in ORAI1 and STIM1. *Annals of the New York Academy of Sciences* 1356:45-79

25. Lee TE, Yu L, Wolf MJ, Rockman HA. 2014. Galactokinase is a novel modifier of calcineurin-induced cardiomyopathy in Drosophila. *Genetics* 198:591-603

26. Lin N, Badie N, Yu L, Abraham D, Cheng H, et al. 2011. A method to measure myocardial calcium handling in adult Drosophila. *Circulation research* 108:1306-15

27. Luo X, Hojayev B, Jiang N, Wang ZV, Tandan S, et al. 2012. STIM1-dependent store-operated Ca(2)(+) entry is required for pathological cardiac hypertrophy. *Journal of molecular and cellular cardiology* 52:136-47

28. Maillet M, van Berlo JH, Molkentin JD. 2013. Molecular basis of physiological heart growth: fundamental concepts and new players. *Nature reviews. Molecular cell biology* 14:38-48

29. Makarewich CA, Zhang H, Davis J, Correll RN, Trappanese DM, et al. 2014. Transient receptor potential channels contribute to pathological structural and functional remodeling after myocardial infarction. *Circulation research* 115:567-80

30. Mattei AL, Riccio ML, Avila FW, Wolfner MF. 2015. Integrated 3D view of postmating responses by the Drosophila melanogaster female reproductive tract, obtained by micro-computed tomography scanning. *Proceedings of the National Academy of Sciences of the United States of America* 112:8475-80

31. Mazurek JA, Jessup M. 2017. Understanding Heart Failure. *Heart failure clinics* 13:1-19

32. McKenna WJ, Maron BJ, Thiene G. 2017. Classification, Epidemiology, and Global Burden of Cardiomyopathies. *Circulation research* 121:722-30

33. McMullen JR, Jennings GL. 2007. Differences between pathological and physiological cardiac hypertrophy: novel therapeutic strategies to treat heart failure. *Clinical and experimental pharmacology & physiology* 34:255-62

34. Mizutani R, Saiga R, Takeuchi A, Uesugi K, Suzuki Y. 2013. Three-dimensional network of Drosophila brain hemisphere. *Journal of structural biology* 184:271-9

35. Mizutani R, Takeuchi A, Akamatsu G, Uesugi K, Suzuki Y. 2008. Element-specific microtomographic imaging of Drosophila brain stained with high-Z probes. *Journal of synchrotron radiation* 15:374-7

36. Molkentin JD, Lu JR, Antos CL, Markham B, Richardson J, et al. 1998. A calcineurin-dependent transcriptional pathway for cardiac hypertrophy. *Cell* 93:215-28

37. Monier B, Astier M, Sémériva M, Perrin L. 2005. Steroid-dependent modification of Hox function drives myocyte reprogramming in the Drosophila heart. *Development (Cambridge, England)* 132:5283

38. Nguyen N, Biet M, Simard É, Béliveau É, Francoeur N, et al. 2013. STIM1 participates in the contractile rhythmicity of HL-1 cells by moderating T-type Ca2+ channel activity. *Biochimica et Biophysica Acta (BBA) - Molecular Cell Research* 1833:1294-303

39. Ocorr K, Perrin L, Lim HY, Qian L, Wu X, Bodmer R. 2007. Genetic control of heart function and aging in Drosophila. *Trends in cardiovascular medicine* 17:177-82

40. Ocorr K, Vogler G, Bodmer R. 2014. Methods to assess Drosophila heart development, function and aging. *Methods (San Diego, Calif.)* 68:265-72

41. Ohba T, Watanabe H, Murakami M, Sato T, Ono K, Ito H. 2009. Essential role of STIM1 in the development of cardiomyocyte hypertrophy. *Biochemical and biophysical research communications* 389:172-6

42. Park CY, Shcheglovitov A, Dolmetsch R. 2010. The CRAC channel activator STIM1 binds and inhibits L-type voltage-gated calcium channels. *Science (New York, N.Y.)* 330:101-5

43. Parks C, Alam MA, Sullivan R, Mancarella S. 2016. STIM1-dependent Ca(2+) microdomains are required for myofilament remodeling and signaling in the heart. *Scientific reports* 6:25372

44. Petersen CE, Wolf MJ, Smyth JT. 2020. Suppression of store-operated calcium entry causes dilated cardiomyopathy of the Drosophila heart. *Biol Open* 9

45. Piazza N, Wessells RJ. 2011. Drosophila models of cardiac disease. *Progress in molecular biology and translational science* 100:155-210

46. Putney JW. 2011. The physiological function of store-operated calcium entry. *Neurochemical research* 36:1157-65

47. Rotstein B, Paululat A. 2016. On the Morphology of the Drosophila Heart. *Journal of cardiovascular development and disease* 3

48. Sabourin J, Bartoli F, Antigny F, Gomez AM, Benitah JP. 2016. Transient Receptor Potential Canonical (TRPC)/Orai1-dependent Store-operated Ca2+ Channels: NEW TARGETS OF ALDOSTERONE IN CARDIOMYOCYTES. *The Journal of biological chemistry* 291:13394-409

49. Schoborg TA. 2020. Whole Animal Imaging of Drosophila melanogaster using Microcomputed Tomography. *Journal of visualized experiments : JoVE*

50. Schoborg TA, Smith SL, Smith LN, Morris HD, Rusan NM. 2019. Micro-computed tomography as a platform for exploring Drosophila development. *Development (Cambridge, England)* 146

51. Schulz RA, Yutzey KE. 2004. Calcineurin signaling and NFAT activation in cardiovascular and skeletal muscle development. *Developmental biology* 266:1-16

52. Smyth JT, Hwang SY, Tomita T, DeHaven WI, Mercer JC, Putney JW. 2010. Activation and regulation of store-operated calcium entry. *Journal of cellular and molecular medicine* 14:2337-49

53. Tao Y, Schulz RA. 2007. Heart development in Drosophila. *Seminars in cell & developmental biology* 18:3-15

54. Tham YK, Bernardo BC, Ooi JY, Weeks KL, McMullen JR. 2015. Pathophysiology of cardiac hypertrophy and heart failure: signaling pathways and novel therapeutic targets. *Archives of toxicology* 89:1401-38

55. Troupes CD, Wallner M, Borghetti G, Zhang C, Mohsin S, et al. 2017. Role of STIM1 (Stromal Interaction Molecule 1) in Hypertrophy-Related Contractile Dysfunction. *Circulation research* 121:125-36

56. Vega RB, Bassel-Duby R, Olson EN. 2003. Control of cardiac growth and function by calcineurin signaling. *The Journal of biological chemistry* 278:36981-4

57. Vikhorev PG, Vikhoreva NN. 2018. Cardiomyopathies and Related Changes in Contractility of Human Heart Muscle. *International journal of molecular sciences* 19

58. Voelkers M, Salz M, Herzog N, Frank D, Dolatabadi N, et al. 2010. Orai1 and Stim1 regulate normal and hypertrophic growth in cardiomyocytes. *Journal of molecular and cellular cardiology* 48:1329-34

59. Vogler G, Bodmer R, Akasaka T. 2009. A Drosophila model for congenital heart disease. *Drug Discovery Today: Disease Models* 6:47-54

60. Wilkins BJ, Dai YS, Bueno OF, Parsons SA, Xu J, et al. 2004. Calcineurin/NFAT coupling participates in pathological, but not physiological, cardiac hypertrophy. *Circulation research* 94:110-8

61. Wu QQ, Xiao Y, Yuan Y, Ma ZG, Liao HH, et al. 2017. Mechanisms contributing to cardiac remodelling. *Clinical science (London, England : 1979)* 131:2319-45

62. Xu P, Damschroder D, Zhang M, Ryall KA, Adler PN, et al. 2019. Atg2, Atg9 and Atg18 in mitochondrial integrity, cardiac function and healthspan in Drosophila. *Journal of molecular and cellular cardiology* 127:116-24

63. Yu L, Daniels J, Glaser AE, Wolf MJ. 2013. Raf-mediated cardiac hypertrophy in adult Drosophila. *Disease models & mechanisms* 6:964-76

64. Yu L, Daniels J, Glaser AE, Wolf MJ. 2013. Raf-mediated cardiac hypertrophy in adult Drosophila. *Disease models & mechanisms* 6:964-76

65. Yu L, Daniels JP, Wu H, Wolf MJ. 2015. Cardiac hypertrophy induced by active Raf depends on Yorkie-mediated transcription. *Science signaling* 8:ra13

66. Zhang SL, Yu Y, Roos J, Kozak JA, Deerinck TJ, et al. 2005. STIM1 is a Ca2+ sensor that activates CRAC channels and migrates from the Ca2+ store to the plasma membrane. *Nature* 437:902-5

67. Zhao G, Li T, Brochet DX, Rosenberg PB, Lederer WJ. 2015. STIM1 enhances SR Ca2+ content through binding phospholamban in rat ventricular myocytes. *Proceedings of the National Academy of Sciences of the United States of America* 112:E4792-801

68. Zheng H, Zhou M-H, Hu C, Kuo E, Peng X, et al. 2013. Differential roles of the C and N termini of Orai1 protein in interacting with stromal interaction molecule 1 (STIM1) for Ca2+ release-activated Ca2+ (CRAC) channel activation. *The Journal of biological chemistry* 288:11263-72

Figure 1

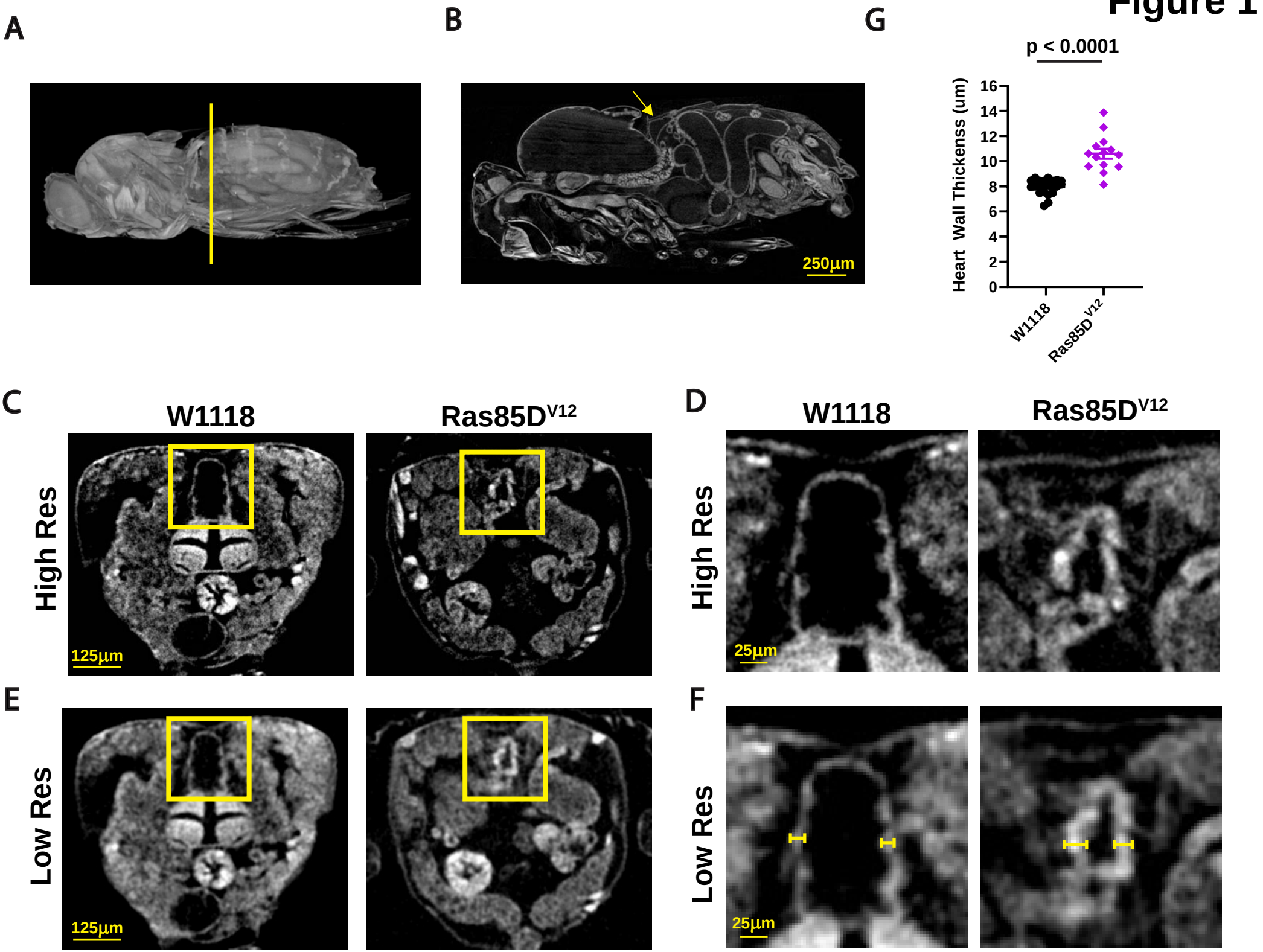
A
B
250µm
G
p < 0.0001
Heart Wall Thickenss (um)
16
14
12
10
8
6
4
2
0
W1118
Ras85D V12
C
W1118
Ras85D V12
High Res
125µm
D
W1118
Ras85D V12
High Res
25µm
E
Low Res
125µm
F
Low Res
25µm

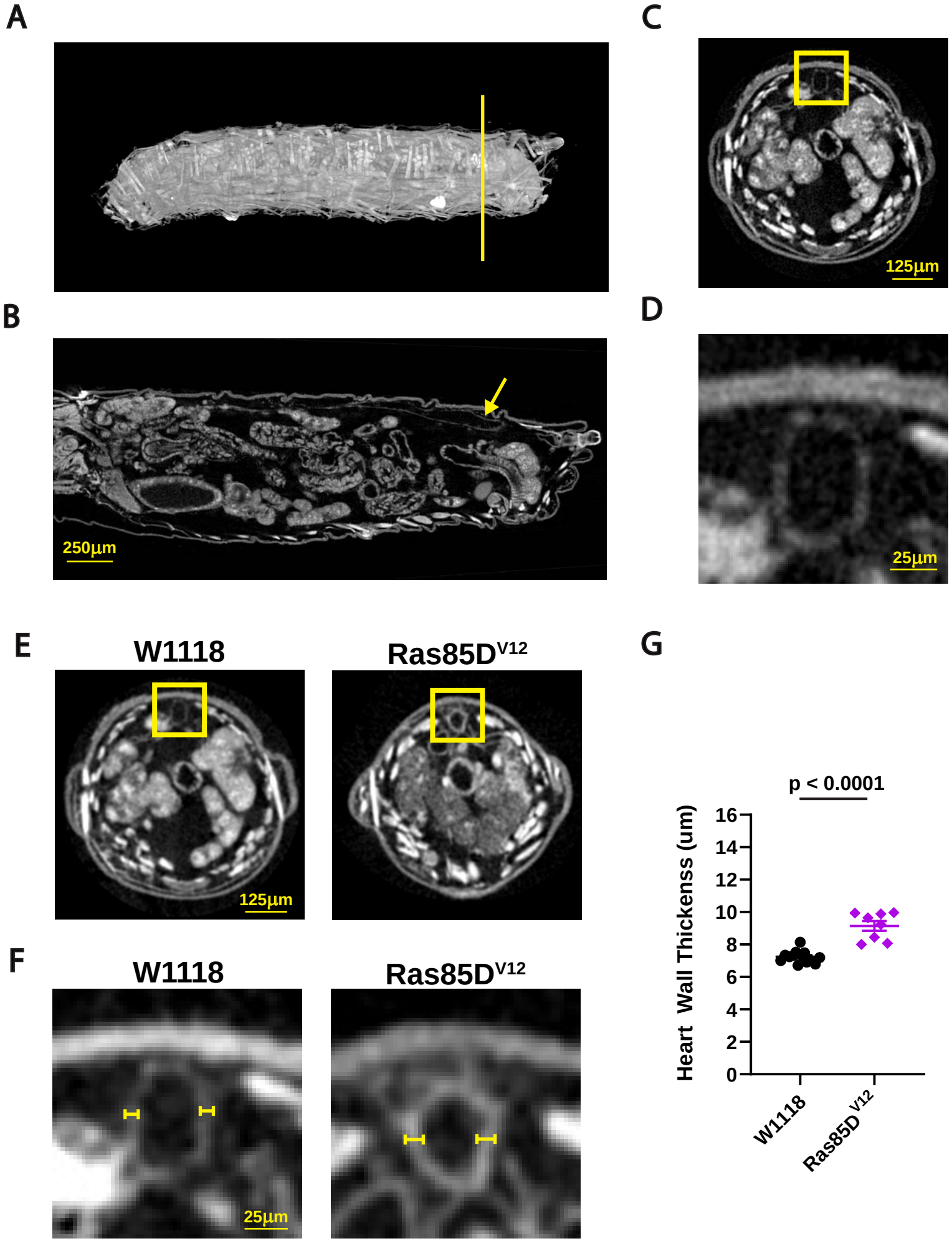
A
B
250µm
C
125µm
D
25µm
E
W1118
Ras85D^{V12}
125µm
F
W1118
Ras85D^{V12}
25µm
G
p < 0.0001
Heart Wall Thickenss (um)
16
14
12
10
8
6
4
2
0
W1118
Ras85D ^{V12}

Figure 2

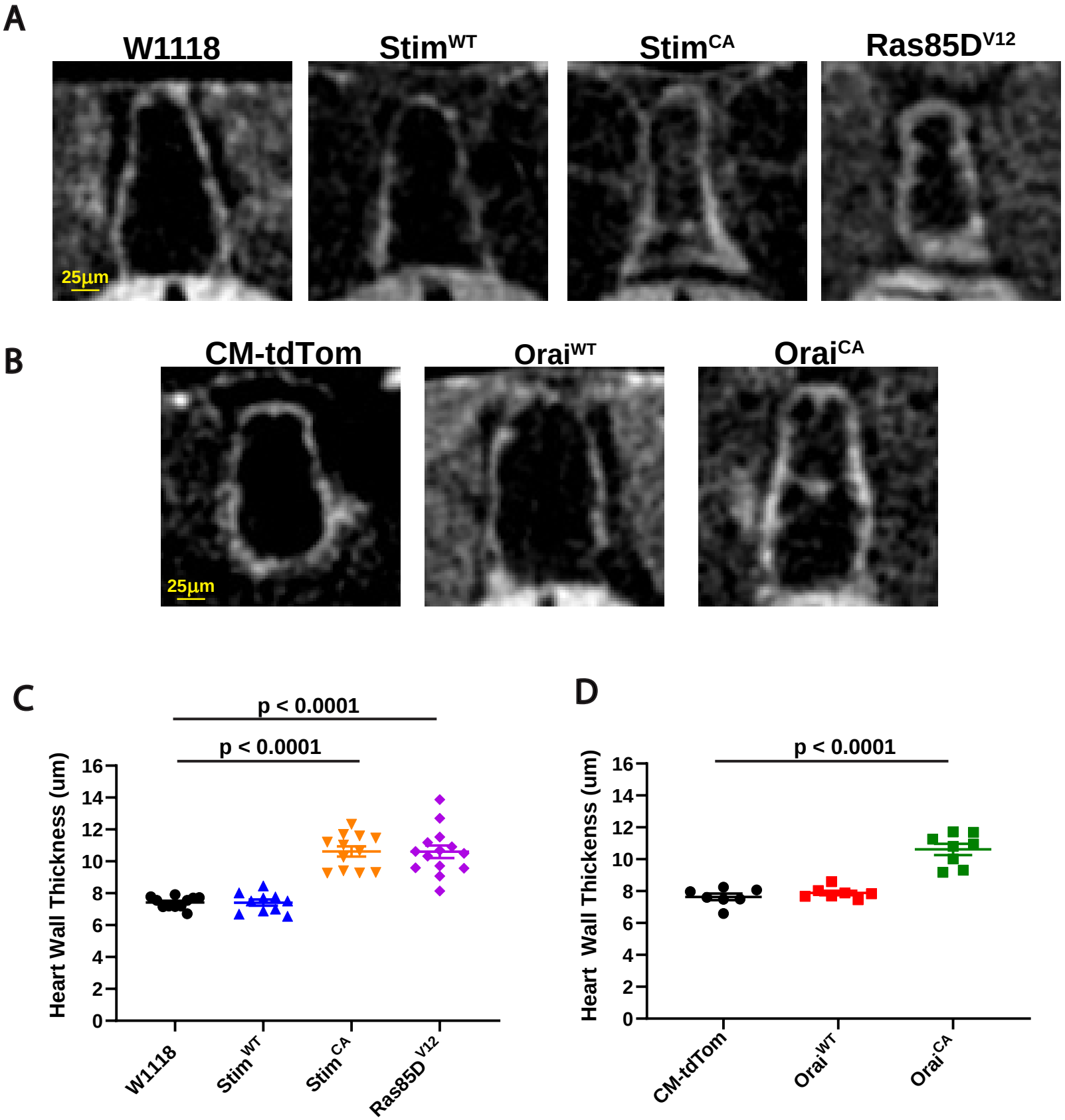
A
W1118
Stim^WT
Stim^CA
Ras85D^V12
25µm
B
CM-tdTom
Orai^WT
Orai^CA
25µm
C
p < 0.0001
p < 0.0001
Heart Wall Thickness (um)
0
2
4
6
8
10
12
14
16
W1118
Stim^WT
Stim^CA
Ras85D^V12
D
p < 0.0001
Heart Wall Thickenss (um)
0
2
4
6
8
10
12
14
16
CM-tdTom
Orai^WT
Orai^CA

Figure 3

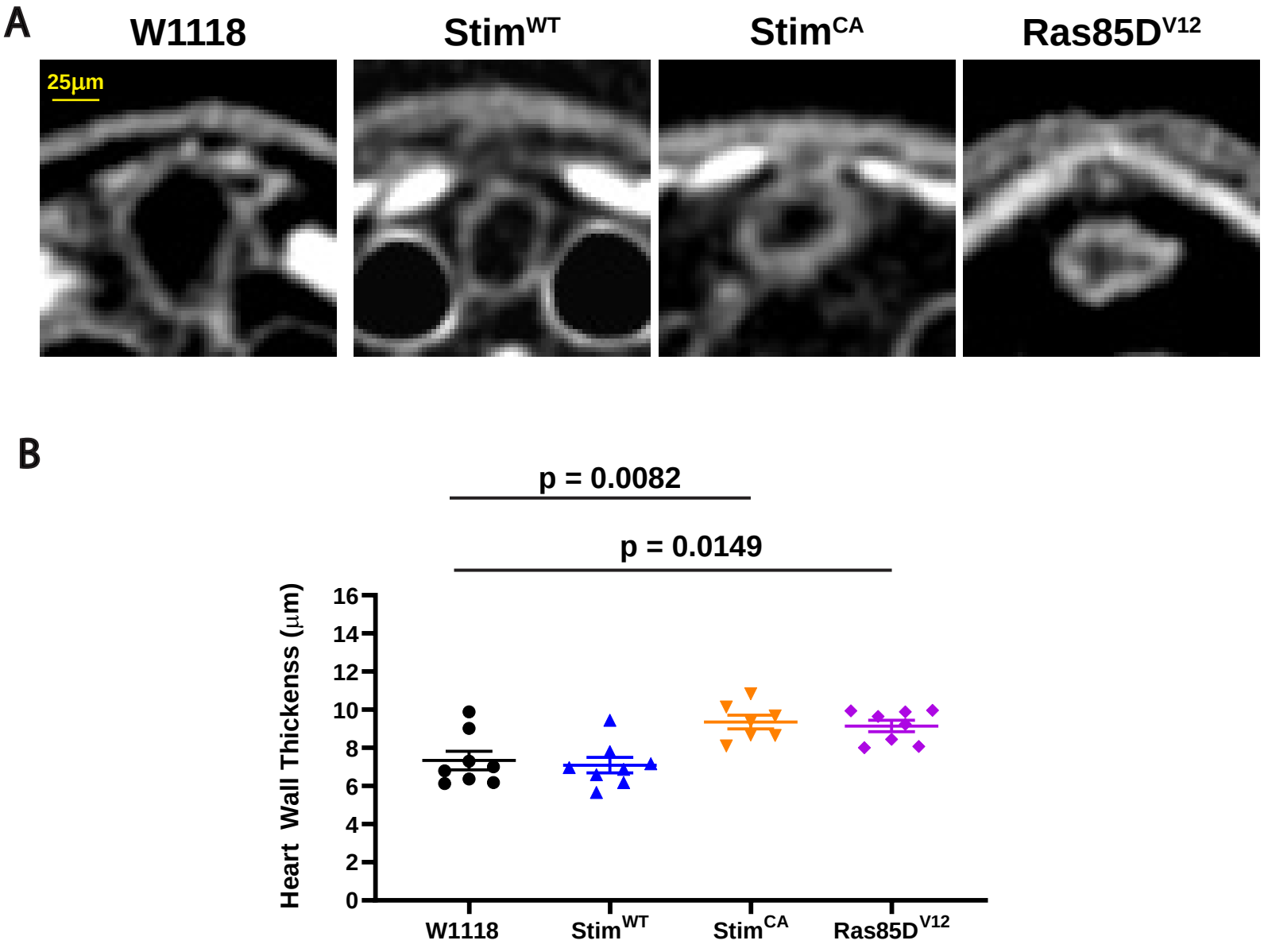
A
W1118
Stim^WT
Stim^CA
Ras85D^V12
25µm
B
p = 0.0082
p = 0.0149
Heart Wall Thickenss (µm)
16
14
12
10
8
6
4
2
0
W1118
Stim^WT
Stim^CA
Ras85D^V12

Figure 4

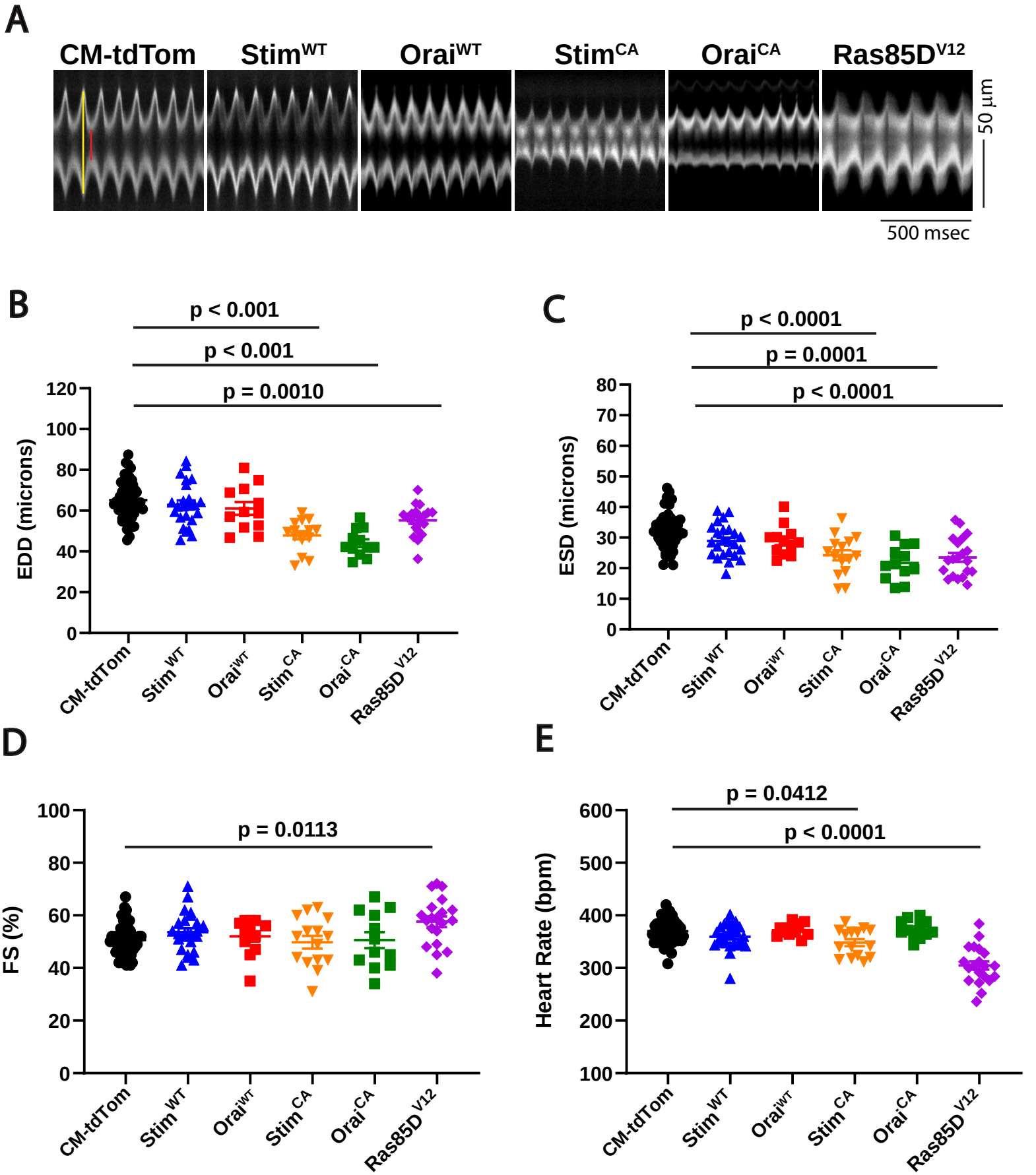
A
CM-tdTom
Stim^WT
Orai^WT
Stim^CA
Orai^CA
Ras85D^V12
50 µm
500 msec
B
p < 0.001
p < 0.001
p = 0.0010
EDD (microns)
C
p < 0.0001
p = 0.0001
p < 0.0001
ESD (microns)
D
p = 0.0113
FS (%)
E
p = 0.0412
p < 0.0001
Heart Rate (bpm)

Figure 5

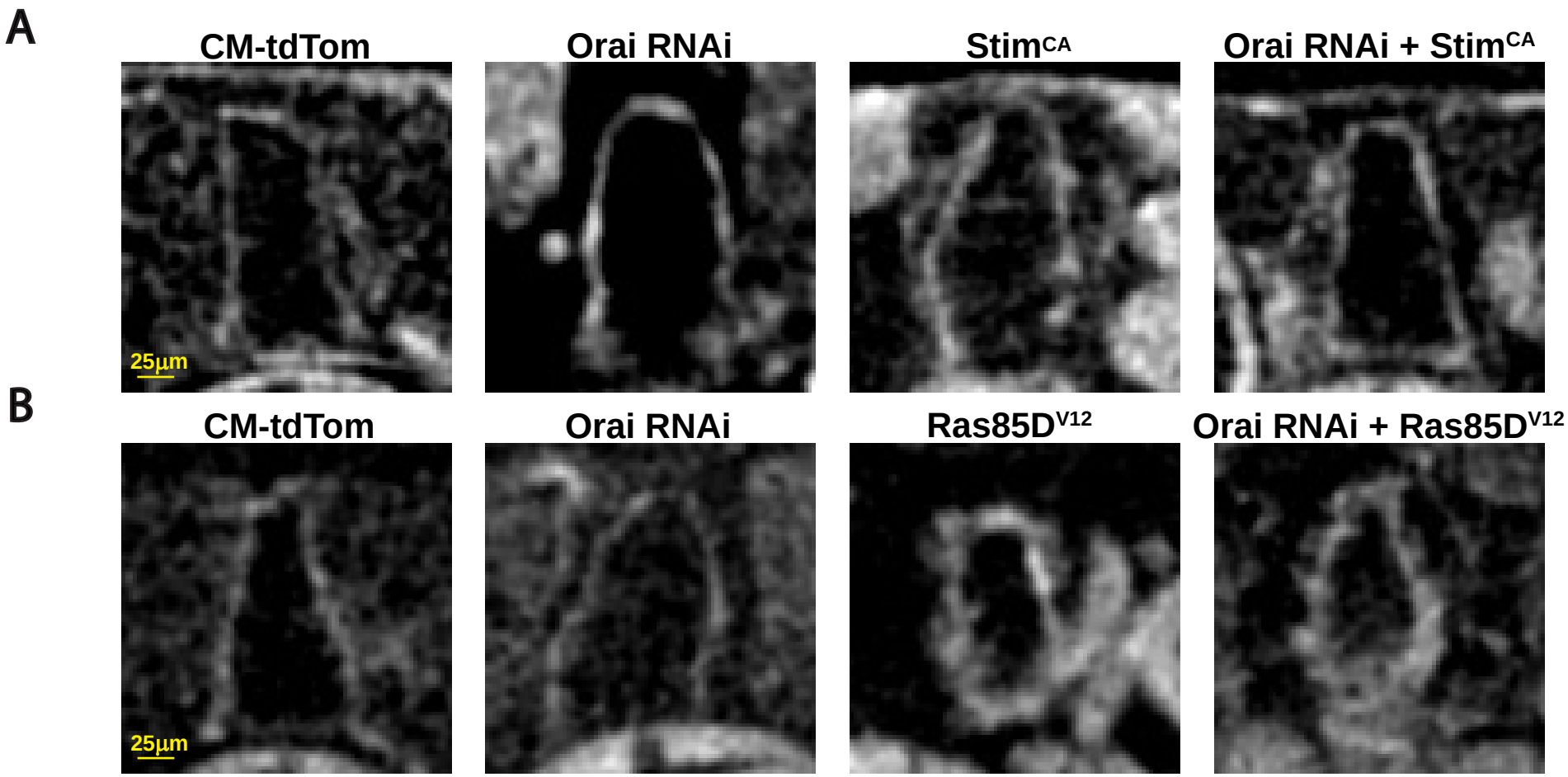
A
CM-tdTom
Orai RNAi
Stim^{CA}
Orai RNAi + Stim^{CA}
25µm
B
CM-tdTom
Orai RNAi
Ras85D^{V12}
Orai RNAi + Ras85D^{V12}
25µm

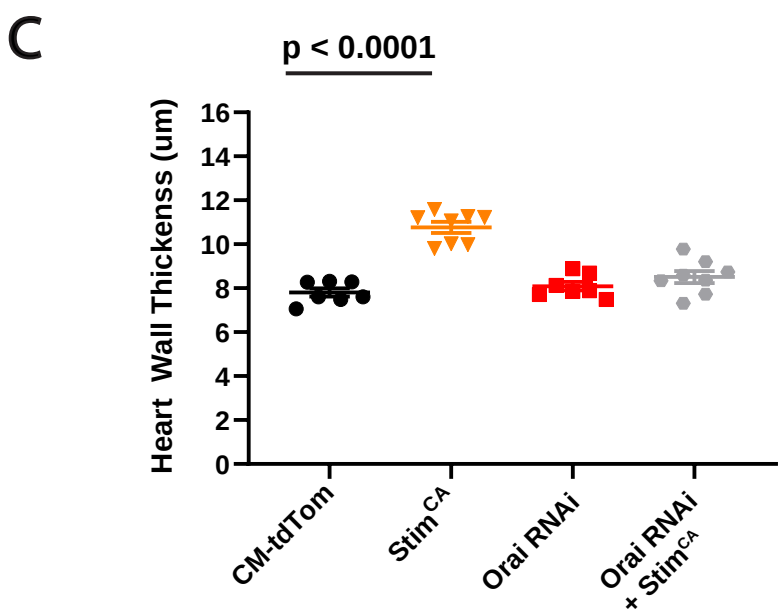
C
p < 0.0001
Heart Wall Thickenss (um)
0
2
4
6
8
10
12
14
16
CM-tdTom
Stim^{CA}
Orai RNAi
Orai RNAi + Stim^{CA}

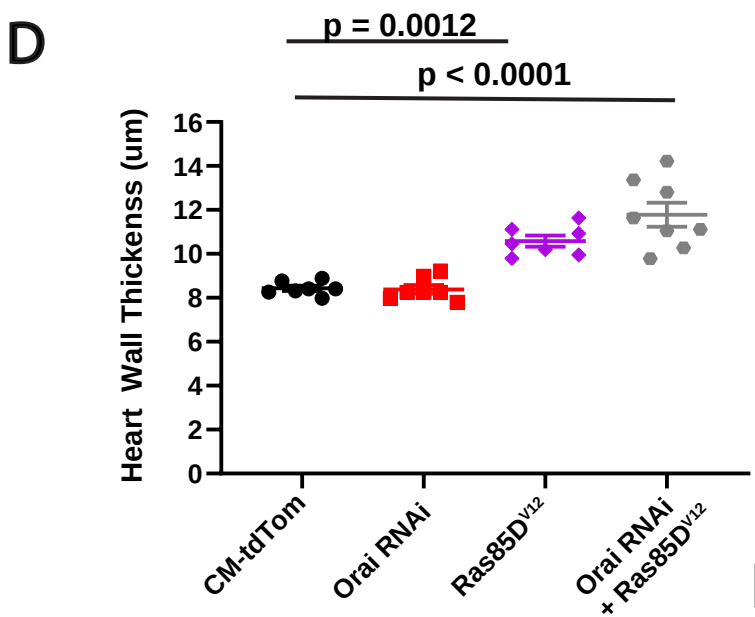
D
p = 0.0012
p < 0.0001
Heart Wall Thickenss (um)
0
2
4
6
8
10
12
14
16
CM-tdTom
Orai RNAi
Ras85D^{V12}
Orai RNAi + Ras85D^{V12}

Figure 6

Figure 7

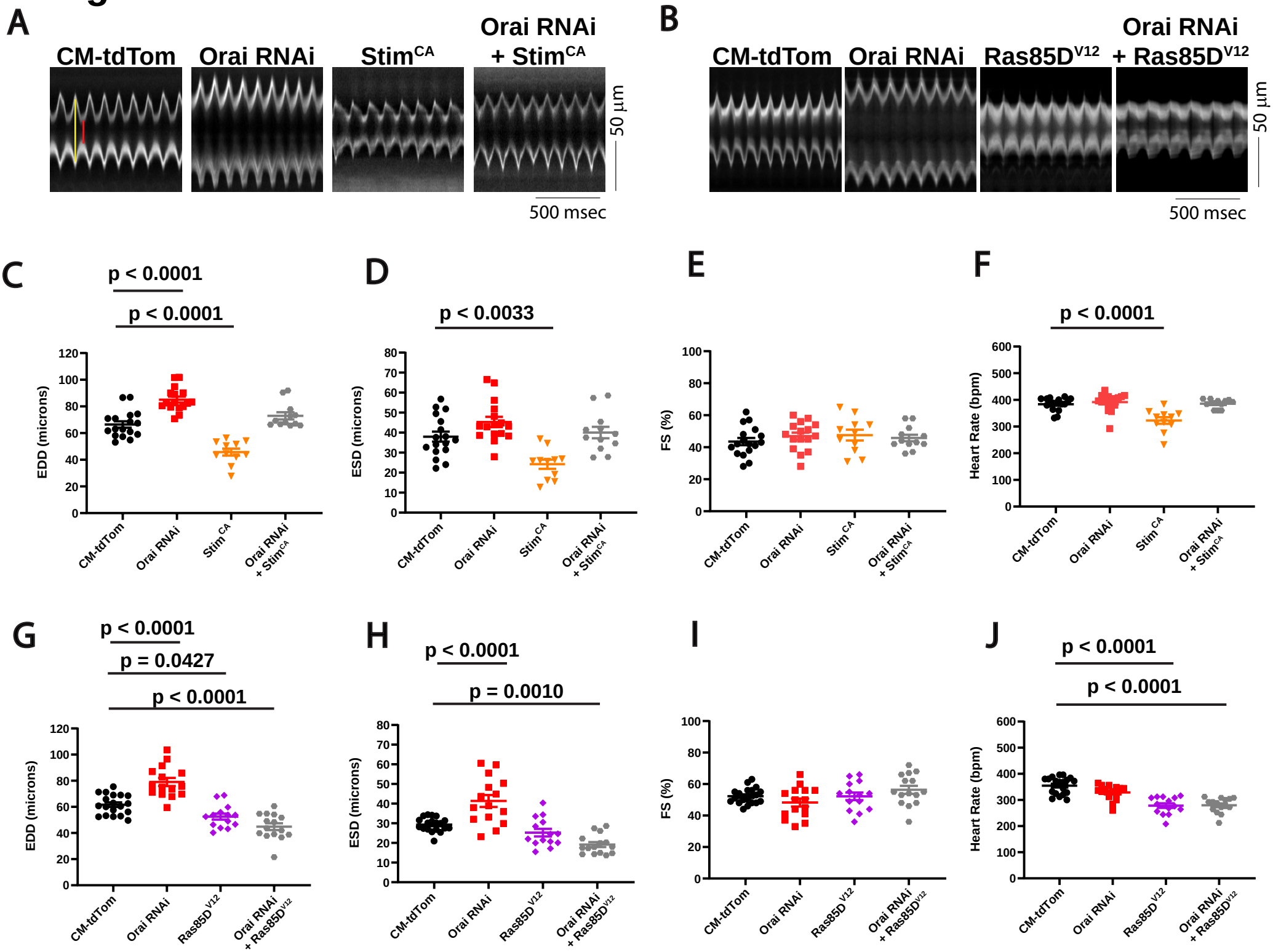
A
CM-tdTom
Orai RNAi
Stim^{CA}
Orai RNAi + Stim^{CA}
50 µm
500 msec
B
CM-tdTom
Orai RNAi
Ras85D^{V12}
Orai RNAi + Ras85D^{V12}
50 µm
500 msec
C
p < 0.0001
p < 0.0001
EDD (microns)
D
p < 0.0033
ESD (microns)
E
FS (%)
F
p < 0.0001
Heart Rate (bpm)
G
p < 0.0001
p = 0.0427
p < 0.0001
EDD (microns)
H
p < 0.0001
p = 0.0010
ESD (microns)
I
FS (%)
J
p < 0.0001
p < 0.0001
Heart Rate (bpm)
CM-tdTom
Orai RNAi
Stim^{CA}
Orai RNAi + Stim^{CA}
Ras85D^{V12}
Orai RNAi + Ras85D^{V12}